JACS
JOURNAL OF THE AMERICAN CHEMICAL SOCIETY

Article

pubs.acs.org/JACS

Tunable Photothermal Actuators Based on a Pre-programmed Aligned Nanostructure

Jue Deng, Jianfeng Li, Peining Chen, Xin Fang, Xuemei Sun, Yishu Jiang, Wei Weng, Bingjie Wang, and Huisheng Peng*

State Key Laboratory of Molecular Engineering of Polymers, Department of Macromolecular Science and Laboratory of Advanced Materials, Fudan University, Shanghai 200438, China

Supporting Information

ABSTRACT: For various applications, it is challenging but essential to obtain complex tunable mechanical actuations in response to environmental stimuli. Here, a general and effective strategy is developed to produce multiple types of photomechanical actuation (from phototropic/apheliotropic bending to three-dimensional helical buckling) by manipulating the orientation of one-dimensional nanomaterials. These materials are manipulated to mimic plants that generate diverse mechanical motions through the orientation of cellulose fibrils. The photomechanical actuations can be completed in milliseconds and can be performed reversibly without detectable fatigue after 100 000 cycles. This capacity to produce multiple types of photomechanical actuation is further developed to produce complex integrated movements, as demonstrated by a light-manipulated robotic arm and a solar energy harvesting system.

INTRODUCTION

By organizing their microscopic structures, plants are able to generate diverse mechanical motions in response to external stimuli.[1−5] For instance, hygroscopic seed dispersal, a type of plant motion, consists of a variety of deformations that share a similar structure and mechanism.[6−8] The orientation of cellulose fibrils embedded in a matrix of hemicellulose, lignin, pectin, and structural proteins plays a key role in such an actuation, e.g., two-dimensional opening movement in pine cones and three-dimensional twisting motion in *Bauhinia variegata* pods (Figure 1a,b).[3,6,7] Improved understanding of the structure-response relationships in plants has inspired increasing interest in the synthesis of mechanically responsive materials with diverse actuation forms that resemble these biological structures.

Attempts have been made to realize diverse tunable mechanical motions[9−17] by utilizing the stress change in the inorganic film across the phase transition[11] and by embedding molecular switches into liquid crystalline polymers.[12−14] The microactuators on the basis of the inorganic phase transition typically displayed low displacements.[11,18] Inaccessible ultraviolet or infrared regions and rigorous chemical composition requirements have limited the application of liquid crystalline polymers.[9,15] In contrast, the visible light offers easy access and convenience for operation and represents an ideal stimulus. Increasing attention has also been paid to replicating permeation and dehydration in plants.[19−22] For example, oriented reinforcing microplatelets have been embedded into a humidity responsive hydrogel,[20] and a hydrogel sheet has been designed with periodic strips of different compositions to demonstrate self-shaping.[21] However, it is difficult to rapidly and accurately tune such humidity-sensing materials, and remote manipulation is not possible.

Here, we present a general strategy that is effective for fabricating visible-light-responsive actuators with diverse and tunable deformations by embedding aligned carbon nanotubes (CNTs) in paraffin wax on a polyimide substrate. The aligned CNTs function as cellulose fibrils, and the paraffin wax resembles the soft cells/tissues of a plant. Photomechanical actuations from phototropic/apheliotropic bending to three-dimensional helical buckling are controlled by tuning the CNT alignment direction. In addition to serving as a geometrical constraint element, the aligned CNTs also enable to absorb infrared and visible light, endowing the resultant actuators with rapid responsiveness. These photomechanical actuators are assembled into a mechanical arm and an energy harvesting system to execute complex but well-controlled motions.

RESULTS AND DISCUSSION

To fabricate the tunable visible-light-driven actuator, paraffin wax was melted and then spin-coated onto a commercial Kapton film, followed by paving multiple layers of aligned CNTs (Figure S1). The composite film was subsequently reheated to promote the embedding of the aligned CNTs into the molten paraffin wax (Experimental Section). Importantly,

Received: October 1, 2015
Published: December 17, 2015

DOI: 10.1021/jacs.5b10131
J. Am. Chem. Soc. 2016, 138, 225−230

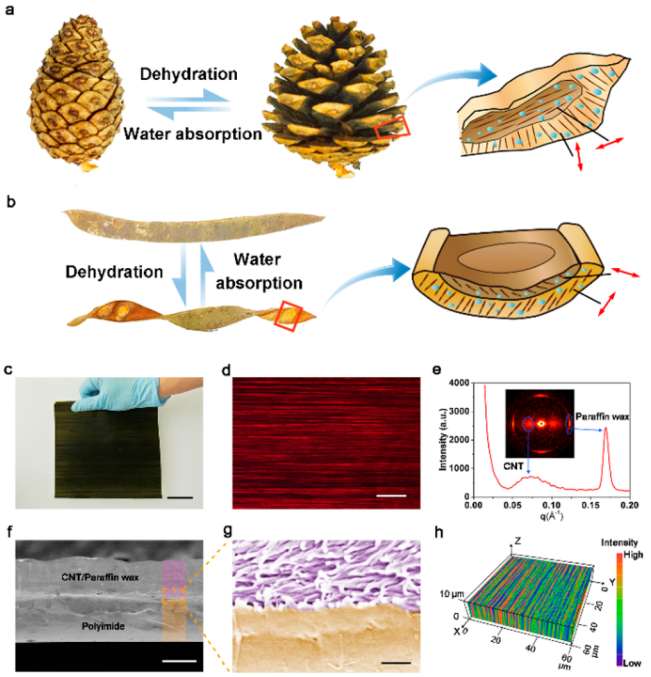

Figure 1. (a) Reversible opening and closing movements of a pine cone and schematic of a cross-sectional active region. (b) Hygroscopic twisting in a *Bauhinia variegata* pod and illustration of the active region, indicating the orientation of cellulose fibrils. (c) Optical image of the as-prepared composite film. (d) Fluorescence image of a paraffin wax/CNT layer, top view. (e) Small-angle X-ray scattering profile (inset, two-dimensional pattern) showing that the CNTs are aligned and the paraffin wax is orientationally crystallized. (f) SEM image at low magnification, side view. (g) Higher magnification of the image in panel f. (h) Three-dimensional confocal microscopy image of the composite film with low and high fluorescence intensities corresponding to CNT and rhodamine-modified paraffin wax, respectively. Scale bars, 5 cm, 200 μm, 10 μm, and 200 nm in c, d, f, and g, respectively.

the composite film could be easily scaled up to meet application requirements. Figure 1c shows a large composite film sheet with a size of 15 cm × 15 cm. The surface of the resultant composite film was smooth, and the aligned CNT structures were well maintained after being embedded into the paraffin wax (Figure 1d,e and Figure S2). The paraffin wax/CNT composite layer and Kapton film were compactly contacted with each other, thereby improving heat transfer and mechanical coherence (Figure 1f,g). In addition, the paraffin wax evenly filled the nanoscale gaps among the aligned CNTs (Figure 1h), producing a structure similar to that of plant cell walls, in which cellulose microfibrils are embedded in the hemicellulose and lignin.[3]

Multiple Photoresponsive Actuation. The composite films were readily cut into strips with different CNT orientations but the same aspect ratio (Figure 2a). Here, we define the strips with transversely aligned and longitudinally aligned CNTs as Strips A and B, respectively. Notably, strips with different CNT orientations produced distinct types of photoresponsive actuation (Figure 2b,c). To quantitatively describe the anisotropy of the composite strips, we define α as the angle between the CNT orientation and the longitudinal direction of the strip (Figure 2a). Unless otherwise specified, the aligned CNT/paraffin wax composite layer (as opposed to the polyimide substrate) was illuminated by visible light with an intensity similar to one sun, or 100 mW cm^{-2}. Therefore, curling motion toward the polyimide substrate or CNT/paraffin wax layer was defined as apheliotropic or phototropic bending, respectively. The photoresponsive actuation was recorded by a digital video camera and investigated using frame-by-frame analysis. Upon irradiation, Strip A (α = 90°) exhibited rapid apheliotropic bending within ~0.87 s, with a bending angle of ~85°; the strip returned to its original state within ~1.86 s after the removal of light (Figure 2b and Movie S1). In comparison, Strip B (α = 0°), in which the CNTs were longitudinally aligned, exhibited phototropic bending within ~1.1 s, with a bending angle of ~60° (Figures 2c and 3a and Movie S2).

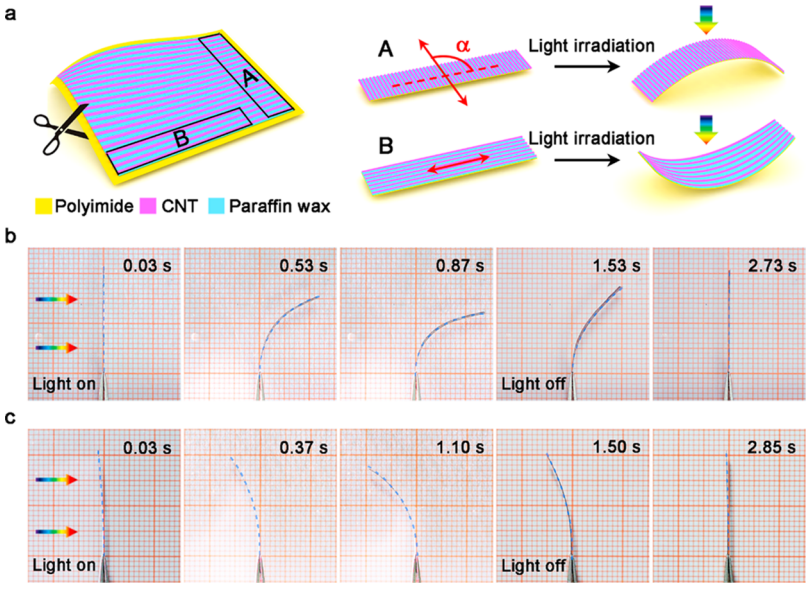

Figure 2. (a) Schematic illustration of the apheliotropic and phototropic bending of the composite strips with different aligned directions of CNTs. (b) Photographs of Strip A (length of 20 mm, width of 4 mm, and thickness of 23 μm) in response to visible light (illuminated from the left, with an intensity of 100 mW cm^{-2}). (c) Photographs of Strip B in response to visible light.

DOI: 10.1021/jacs.5b10131
J. Am. Chem. Soc. 2016, 138, 225−230

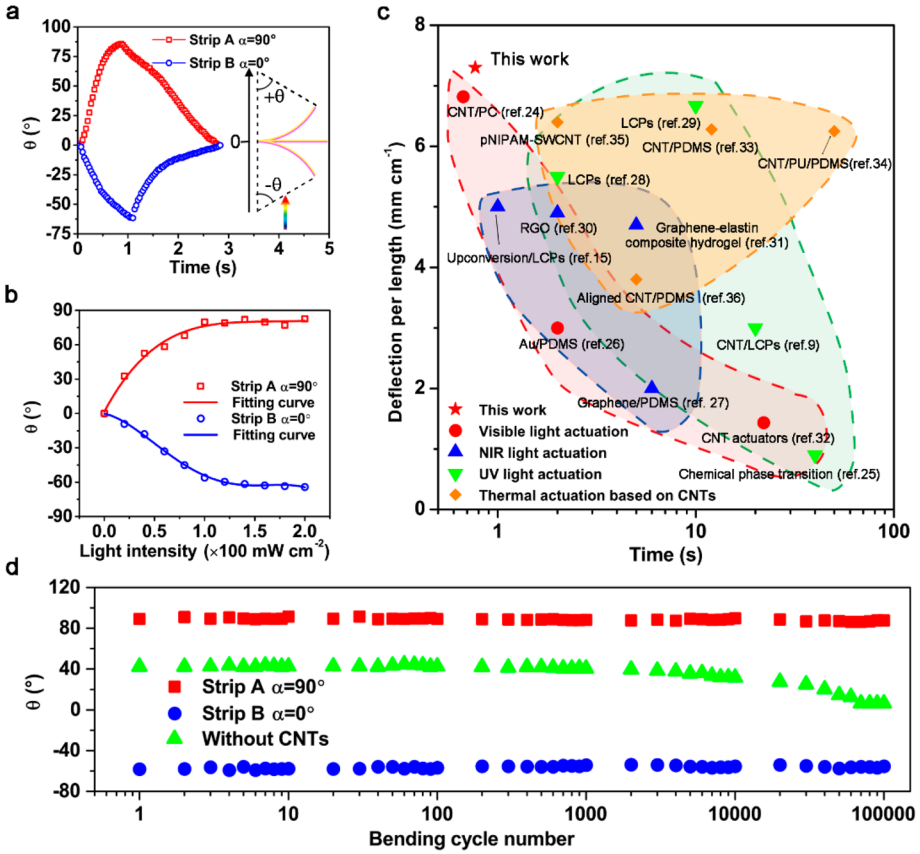

Figure 3. (a) Dependence of the bending angle on the operation time for Strips A and B (inset, schematic illustration of the bending angle). (b) Dependence of the maximal bending angle of Strips A and B on the illumination intensity. (c) Ashby-like plot comparing different light-driven actuation properties. (d) Dependence of the bending angle on the bending cycle number for Strips A and B.

As a result of the high absorption of visible and near-infrared light and efficient thermal transformation of the aligned CNTs,[9,23,24] the magnitudes of bending motion were highly tunable (Figure S3). Specifically, CNTs were able to distinguish different visible light intensities and efficiently converted photonic energy to thermal energy to achieve different levels of deformations (Figure 3b). The near-infrared light (wavelengths >772 nm) also showed the same effect (Figure S3). In addition, tunable manipulation could also be achieved by controlling the percentage of illumination areas and the voids among aligned CNTs, and relatively lower deformations were generated from local illuminations or larger voids (Figures S4 and S5 and note 1.1 in the Supporting Information). The response speed was comparable with—or even superior to—that of typical light-driven actuators[25−32] as well as thermally or electrothermally driven actuators based on CNTs[33−36] (Figure 3c). For instance, these composite materials were one to two magnitudes faster than azobenzene-containing liquid-crystalline elastomers[15,28,29] and faster than graphene-based actuator[27,30,31] and other CNT-based actuators.[32−36] In addition to the substantial light absorption and thermal conduction of the aligned CNTs, the large difference in heat capacity between paraffin wax (~3 K^{-1}) and polyimide (~2.8 × 10^{-5} K^{-1}) (Figures S6 and S7) also contributed to the remarkable deformation.[37] Therefore, the composite strip can hardly generate bending deformation without polyimide substrate. Besides the large coefficient of thermal expansion of paraffin wax, the suitable modulus also contributed to rapid response. If the other polymers such as polydimethylsiloxane were used to replace the paraffin wax, lower deformations and slower responses were observed (Figure S8).

Here the extent of bending was characterize by the deflection per length, and it exceeded most examples of light-driven actuation (Figure 3c). Note that the thinner the actuating film is, the larger distance the actuator produces. For the previous report based on CNTs, the thickness was ~12 μm;[24] this composite strip showed a thickness of 23 μm. The actuation of the composite strip was highly reversible, and no detectable decrease in bending angle was observed, even after 100 000 cycles (Figure 3d). In strong contrast, the temperature of the strips without aligned CNTs was only slightly increased (by less than 5 °C) upon illumination under the same conditions (Figure S9), and the bending angle was considerably lower than that of Strips A or B (Figure S10); the magnitudes of deformation was also severely attenuated. The high stability is attributed to the close contact between polyimide substrate and paraffin wax/CNT layer during deformation (Figure S11). The large specific surface area of CNTs and high compatibility with paraffin wax also prevent the loss of paraffin wax and uneven distribution. Considering that available actuators typically generate unidirectional deformation; in comparison, the opposite bending directions of Strips A and B—which use the same components—are unusual. They differ only in the different orientation directions of the aligned CNTs. The composite strips were suitably controlled by varying the α angles for varied actuations; for example, right- and left-handed helical deformations were generated at 45° and 135°, respectively (Figure S12).

DOI: 10.1021/jacs.5b10131
J. Am. Chem. Soc. 2016, 138, 225−230

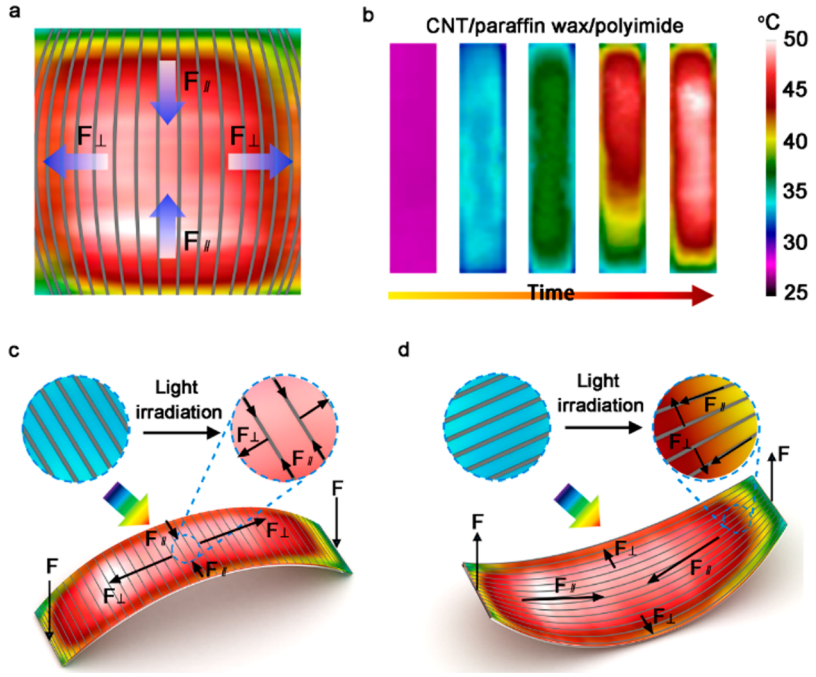

Figure 4. (a) Schematic illustration of the tensile stress and contraction stress in the transverse and longitudinal directions of aligned CNTs under irradiation. (b) Infrared images of a composite strip after irradiation. (c) Schematic illustration of the mechanism of apheliotropic bending. Tensile stress predominates in the longitudinal direction. (d) Schematic illustration of the mechanism of phototropic bending. Contraction stress predominates in the longitudinal direction.

Mechanism of Photoresponsive Actuation. The aligned CNT sheets were anisotropic materials with a high longitudinal modulus but a low transverse modulus,[38] which exerted a geometrical constraint on the expansion of paraffin wax. Because of the constraint of the aligned CNTs, the paraffin wax tended to widen the spaces between CNT bundles and expand perpendicularly in the orientation of aligned CNTs, producing the tensile stress $F_{\perp}$ (Figure 4a). More direct evidence was provided by microscopic observation of the strip without a Kapton substrate upon heating. As the temperature was increased from 5 to 35 °C, the edges of the CNT/paraffin wax composite film extended outward by 28 μm along the transverse direction (Figure S13). In addition, because of the different thermal diffusion rates between the strip and environment, the temperatures at the edges were lower than in the middle after illumination (Figure 4b). Consequently, the edges of the strips extended less than the middle area, which was equivalent to the case of the strip edges being confined. Therefore, a contractile stress ($F_{\parallel}$) appeared in the longitudinal direction as an accompanied effect of expansion in transverse direction (Figure 4a).

The different types of motion in Strips A and B arise from the competition between $F_{\perp}$ and $F_{\parallel}$. However, our experiments showed that the polyimide substrate strongly resisted shearing deformation and that deformation of the strips preserved the Gaussian curvature; as a result, only one of the two bending directions predominated. Considering the large aspect ratios of the strips, the contractile or tensile stress of CNT/paraffin wax composite layer predominated in the longtitudinal direction. In this case, the strains were more easily generated in the longitudinal direction than the transverse direction. Therefore, $F_{\perp}$ along the longitudinal direction of Strip A generated a higher strain than $F_{\parallel}$ exerted by the contractile stress in the transverse direction (Figure 4c). As a result, Strip A exhibited apheliotropic bending. For Strip B, the contractile stress ($F_{\parallel}$) in the longitudinal direction dominated the process, and phototropic bending was observed (Figure 4d).

Theoretical simulations were also carried out to compare minimal free energies and explain the bending direction (note 2 and Figures S14–S16 in the Supporting Information). From a thermodynamic perspective, each infinitesimal region in a strip generated a local spontaneous curvature based on the temperature distribution to minimize free energy. Both Strips A and B exhibited a similar temperature distribution (Figure S17), and the difference between the thermal diffusion rate in the longitudinal and transverse directions was negligible for the dense, multilayer CNT sheets.[39−41] Therefore, the equilibrium shape or competing result of bending directions was determined by free energy minimization. The simulation also predicted that Strip A would exhibit apheliotropic bending, whereas Strip B would exhibit phototropic bending (Figure S15).

To verify our assumption that the photoresponsive actuation behavior of the composite strip arose from the thermal expansion of the paraffin wax, we examined the heating effect alone on the actuation behavior of the same composite strip. As expected, Strip A underwent the same bending direction as that under irradiation, and the bending curvature reached ~60° when the temperature was increased to 40 °C, which is consistent with the deformation generated by irradiation (Figure S18). In contrast, Strip A underwent the opposite deformation because paraffin wax shrank at lower temperature, and decreasing the temperature did not reduce the modulus of the composite layer that inversely occurred at high temperature. As Strip A approached the surface of the liquid nitrogen, the flat strip deformed into a closed ring (Figure S19). Furthermore, we had designed the composite strips with different orientations. As expected, the composite strips produced

DOI: 10.1021/jacs.5b10131
J. Am. Chem. Soc. 2016, 138, 225−230

different three-dimensional helices by varying α from 30 to 45, 60, or 90° (Figures S19 and S20, and Movie S3), which was mainly governed by the contractile stress perpendicularly in the orientation of aligned CNTs. The slope angle of the deformed helix corresponded to the predefined value of α.

Applications of Actuators. A light-manipulated mechanical arm was assembled to demonstrate the capability of varied and tunable actuations. The telescopic arm was first fabricated from a preshaped helical Strip B. The resulting helix was responsive to visible light, following the same mechanism described above. Upon irradiation, it executed a rapid untwisting transformation accompanied by an elongation in length and subsequently remained in a tensional state until the light was switched off (Figure 5a,b and Movie S4). Upon

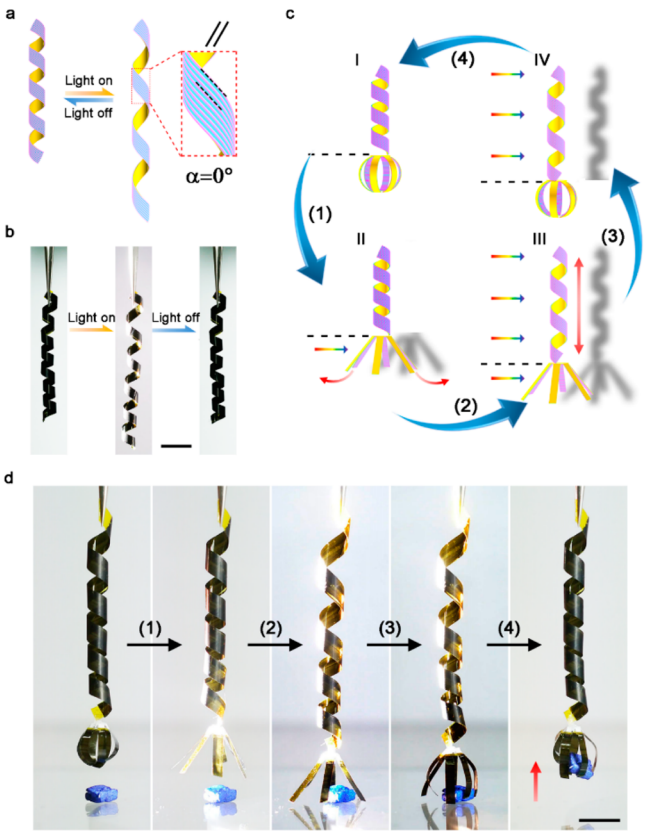

Figure 5. (a) Schematic illustration of helical Strip B. (b) Photographs of helical Strip B before and after light irradiation. (c) Schematic illustration of a mechanical arm in four states: (1) the claw being opened, (2) the arm being elongated, (3) the claw being closed, and (4) the arm being contracted. When the four states are anticlockwise (clockwise) cycled from I to IV, the mechanical arm completes a catching (releasing) movement. (d) Photographs of an object being lifted up by the mechanical arm. Scale bars, 1 cm in b and d.

removal of the visible light, helical Strip B returned to its original state. In contrast, helical Strip A displayed a twisting and lengthwise constriction under illumination (Figure S21 and Movie S5). Strips A and B were both shaped into left-hand helices through a thermal treatment, and their response was unaffected by chirality; rather, their helical motion was determined only by the microscopic configuration.

The maximum elongation/contraction of helical Strips A and B were ~120% and 80%, respectively. Both twisting and untwisting deformations were rapidly produced (~1.2 s) and were highly reversible (Figure S22). For helical Strip B, the rotation angle reached ~550°, and the maximum rotation speed for untwisting was ~250 rotations per minute (rpm) (Figure S23). The theoretical simulation predictions were also consistent with the elongation deformation of helical Strip B.

Six Strip A specimens were connected to the end of a helical Strip B to serve as a claw. This mechanical arm was able to conduct grasping/releasing and elongation/contraction movements manipulated by illuminated areas; the four-step movements of the mechanical arm are shown in Figure 5c. Upon illumination, the claw opened and the telescopic arm elongated (II and III). When the light was removed, the claw grasped and clenched an object (IV), and the telescopic arm contracted and lifted the object up (I) (Figure 5d and Movie S6). Provided that the light was manipulated inversely, the object was gently released to the original position. The rapid response and light sensitivity of the composite actuator thus endow the mechanical arm with real-time and remote controllability, which are desirable in various fields.

Moreover, benefiting from the electrical conductivity of the aligned CNT sheet, the photoresponsive actuator offers great potential in the field of electronic devices. Here, we integrated fiber-shaped perovskite solar cells with actuators to assemble a solar energy-harvesting system. Benefiting from the availability of small and lightweight fiber-shaped solar cells, the photoresponsive behavior of the actuator was slightly affected. As illustrated in Figure S24a, several fiber-shaped solar cells were fixed and serially connected to the composite actuator. The solar cell panels were fixed on a cabin roof (Figure S24b). When the sunlight illuminated the roof, the panels automatically opened, and the solar cells converted the light energy into sufficient electricity to power light emitting diodes (Figure S24c and Movie S7). These intelligent solar cell panels have potential use in a variety of fields, such as mechanical engineering and intelligent electronics.

CONCLUSIONS

In summary, we created a series of tunable photoresponsive actuators with a facile and industry-accessible fabrication process by applying the principle of motion in biological systems. Multiple types of deformation were demonstrated, from two-dimensional phototropic/apheliotropic bending to three-dimensional helical transformations, all of them guided by pre-programmed nanoscale structures. The orientation of the aligned CNTs exerts a geometrical constraint and plays a critical role in modulating photomechanical actuation. Our new understanding of the mechanism prompts application of the same fabrication strategy with other materials that exhibit differential and anisotropic swelling; it also provides a guideline for designing more complex motion, such as helical actuation with twisting/untwisting and elongation/contraction deformation capability. These photomechanical actuators can be integrated to produce novel multi-functional electronic devices.

EXPERIMENTAL SECTION

Fabrication of the Composite Actuator. A commercial Kapton film (polyimide, ~10 μm in thickness) was first paved on the glass substrate, and paraffin wax (Sigma Aldrich 327204) was deposited on the Kapton film and heated to 80 °C. Spin-coating was used to control the mass of paraffin wax on the Kapton film and ensured a uniform distribution; e.g., spinning speeds of 400, 500, 700, 1000, 1500, and 2000 rpm produced area densities of 1.43, 1.15, 0.90, 0.62, 0.40, and 0.30 mg cm^{-2}, respectively. After cooling to room temperature, 20 layers of aligned CNT sheets (~20 nm per layer) were stacked on the

DOI: 10.1021/jacs.5b10131
J. Am. Chem. Soc. 2016, 138, 225−230

uniform paraffin wax layer. The aligned CNT sheets were spun from spinnable CNT arrays that had been synthesized by chemical vapor deposition[39−41] (Figure S1). The CNTs typically showed a diameter of ∼10 nm and length of 250 μm. Finally, the composite film was reheated to 80 °C and then gradually cooled to room temperature. After removal of the glass substrate, the composite actuation film was prepared and cut along different directions, as shown in Figure 2a.

Fabrication of the Helical Actuator and Mechanical Arm. The composite Strips A and B (length of 60 mm and width of 4 mm) were wound on a glass rod with radius of 5 mm with the aligned CNT/paraffin wax composite layer on the outer side. Helical actuators were prepared after a heat treatment at 240 °C in argon for 5 h. For the mechanical arm, six helical Strips A (length of 10 mm and width of 2 mm) were shaped into a bending state through a heat treatment and then assembled to serve as a claw. The helical Strip B acted as a limb.

Fabrication of the Solar Energy Harvesting System. Strip A (length of 70 mm and width of 30 mm) was shaped into a cylinder shape through heat treatment, and five fiber-shaped perovskite solar cells were fixed onto the surface and connected in series by silver paste. To prevent short circuits, the aligned CNT sheets at the contact area between the strip and solar cell were selectively removed prior to integration.

■ ASSOCIATED CONTENT

Supporting Information

The Supporting Information is available free of charge on the ACS Publications website at DOI: 10.1021/jacs.5b10131.

Details of fabrication process, characterization, theoretical simulation, and Figures S1−S24 (PDF)

Movies S1−S7 (ZIP)

■ AUTHOR INFORMATION

Corresponding Author

*penghs@fudan.edu.cn

Notes

The authors declare no competing financial interest.

■ ACKNOWLEDGMENTS

This work was financially supported by NSFC (21225417, 21474021, 21534002), MOST (2011CB932503), STCSM (12 nm0503200), Fok Ying Tong Education Foundation, the Program for Professor of Special Appointment at Shanghai Institutions of Higher Learning, and the Program for Outstanding Young Scholars from Organization Department of the CPC Central Committee.

■ REFERENCES

(1) Fratzl, P.; Barth, F. G. *Nature* **2009**, *462*, 442.
(2) Studart, A. R. *Angew. Chem., Int. Ed.* **2015**, *54*, 3400.
(3) Dumais, J.; Forterre, Y. *Annu. Rev. Fluid Mech.* **2012**, *44*, 453.
(4) Burgert, I.; Fratzl, P. *Philos. Trans. R. Soc., A* **2009**, *367*, 1541.
(5) Egan, P.; Sinko, R.; LeDuc, P. R.; Keten, S. *Nat. Commun.* **2015**, *6*, 7418.
(6) Dawson, C.; Vincent, J. F.; Rocca, A. M. *Nature* **1997**, *390*, 668.
(7) Armon, S.; Efrati, E.; Kupferman, R.; Sharon, E. *Science* **2011**, *333*, 1726.
(8) Elbaum, R.; Zaltzman, L.; Burgert, I.; Fratzl, P. *Science* **2007**, *316*, 884.
(9) Sun, X.; Wang, W.; Qiu, L.; Guo, W.; Yu, Y.; Peng, H. *Angew. Chem., Int. Ed.* **2012**, *51*, 8520.
(10) Wang, W.; Sun, X.; Wu, W.; Peng, H.; Yu, Y. *Angew. Chem., Int. Ed.* **2012**, *51*, 4644.
(11) Wang, T.; Torres, D.; Fernández, F. E.; Green, A. J.; Wang, C.; Sepúlveda, N. *ACS Nano* **2015**, *9*, 4371.
(12) Yu, Y.; Nakano, M.; Ikeda, T. *Nature* **2003**, *425*, 145.
(13) de Haan, L. T.; Gimenez-Pinto, V.; Konya, A.; Nguyen, T. S.; Verjans, J.; Sánchez-Somolinos, C.; Selinger, J. V.; Selinger, R. L.; Broer, D. J.; Schenning, A. P. *Adv. Funct. Mater.* **2014**, *24*, 1251.
(14) Iamsaard, S.; Aßhoff, S. J.; Matt, B.; Kudernac, T.; Cornelissen, J. J.; Fletcher, S. P.; Katsonis, N. *Nat. Chem.* **2014**, *6*, 229.
(15) Wu, W.; Yao, L.; Yang, T.; Yin, R.; Li, F.; Yu, Y. *J. Am. Chem. Soc.* **2011**, *133*, 15810.
(16) Zhao, Q.; Dunlop, J. W.; Qiu, X.; Huang, F.; Zhang, Z.; Heyda, J.; Dzubiella, J.; Antonietti, M.; Yuan, J. *Nat. Commun.* **2014**, *5*, 4293.
(17) Zhao, Q.; Heyda, J.; Dzubiella, J.; Täuber, K.; Dunlop, J. W.; Yuan, J. *Adv. Mater.* **2015**, *27*, 2913.
(18) Cabrera, R.; Merced, E.; Dávila, N.; Fernández, F. E.; Sepúlveda, N. *Microelectron. Eng.* **2011**, *88*, 3231.
(19) Ma, M.; Guo, L.; Anderson, D. G.; Langer, R. *Science* **2013**, *339*, 186.
(20) Erb, R. M.; Sander, J. S.; Grisch, R.; Studart, A. R. *Nat. Commun.* **2013**, *4*, 1712.
(21) Wu, Z. L.; Moshe, M.; Greener, J.; Therien-Aubin, H.; Nie, Z.; Sharon, E.; Kumacheva, E. *Nat. Commun.* **2013**, *4*, 1586.
(22) Thérien-Aubin, H. l.; Wu, Z. L.; Nie, Z.; Kumacheva, E. *J. Am. Chem. Soc.* **2013**, *135*, 4834.
(23) Koerner, H.; Price, G.; Pearce, N. A.; Alexander, M.; Vaia, R. A. *Nat. Mater.* **2004**, *3*, 115.
(24) Zhang, X.; Yu, Z.; Wang, C.; Zarrouk, D.; Seo, J.-W. T.; Cheng, J. C.; Buchan, A. D.; Takei, K.; Zhao, Y.; Ager, J. W.; et al. *Nat. Commun.* **2014**, *5*, 2983.
(25) Sahoo, S. C.; Nath, N. K.; Zhang, L.; Semreen, M. H.; Al-Tel, T. H.; Naumov, P. *RSC Adv.* **2014**, *4*, 7640.
(26) Lan, T.; Hu, Y.; Wu, G.; Tao, X.; Chen, W. *J. Mater. Chem. C* **2015**, *3*, 1888.
(27) Jiang, W.; Niu, D.; Liu, H.; Wang, C.; Zhao, T.; Yin, L.; Shi, Y.; Chen, B.; Ding, Y.; Lu, B. *Adv. Funct. Mater.* **2014**, *24*, 7598.
(28) Yoshino, T.; Kondo, M.; Mamiya, J. i.; Kinoshita, M.; Yu, Y.; Ikeda, T. *Adv. Mater.* **2010**, *22*, 1361.
(29) van Oosten, C. L.; Bastiaansen, C. W.; Broer, D. J. *Nat. Mater.* **2009**, *8*, 677.
(30) Ji, M.; Jiang, N.; Chang, J.; Sun, J. *Adv. Funct. Mater.* **2014**, *24*, 5412.
(31) Wang, E.; Desai, M. S.; Lee, S.-W. *Nano Lett.* **2013**, *13*, 2826.
(32) Lu, S.; Panchapakesan, B. *Nanotechnology* **2005**, *16*, 2548.
(33) Li, Q.; Liu, C.; Lin, Y.-H.; Liu, L.; Jiang, K.; Fan, S. *ACS Nano* **2015**, *9*, 409.
(34) Zeng, Z.; Jin, H.; Zhang, L.; Zhang, H.; Chen, Z.; Gao, F.; Zhang, Z. *Carbon* **2015**, *84*, 327.
(35) Zhang, X.; Pint, C. L.; Lee, M. H.; Schubert, B. E.; Jamshidi, A.; Takei, K.; Ko, H.; Gillies, A.; Bardhan, R.; Urban, J. J.; et al. *Nano Lett.* **2011**, *11*, 3239.
(36) Chen, L.; Liu, C.; Liu, K.; Meng, C.; Hu, C.; Wang, J.; Fan, S. *ACS Nano* **2011**, *5*, 1588.
(37) Lima, M. D.; Li, N.; Jung de Andrade, M.; Fang, S.; Oh, J.; Spinks, G. M.; Kozlov, M. E.; Haines, C. S.; Suh, D.; Foroughi, J.; Kim, S. J.; Chen, Y.; Ware, T.; Shin, M. K.; Machado, L. D.; Fonseca, A. F.; Madden, J. D. W.; Voit, W. E.; Galvão, D. S.; Baughman, R. H. *Science* **2012**, *338*, 928.
(38) Aliev, A. E.; Oh, J.; Kozlov, M. E.; Kuznetsov, A. A.; Fang, S.; Fonseca, A. F.; Ovalle, R.; Lima, M. D.; Haque, M. H.; Gartstein, Y. N.; Zhang, M.; Zakhidov, A. A.; Baughman, R. H. *Science* **2009**, *323*, 1575.
(39) Aliev, A. E.; Guthy, C.; Zhang, M.; Fang, S.; Zakhidov, A. A.; Fischer, J. E.; Baughman, R. H. *Carbon* **2007**, *45*, 2880.
(40) Peng, H.; Sun, X.; Cai, F.; Chen, X.; Zhu, Y.; Liao, G.; Chen, D.; Li, Q.; Lu, Y.; Zhu, Y.; Jia, Q. *Nat. Nanotechnol.* **2009**, *4*, 738.
(41) Qiu, L.; Sun, X.; Guo, W.; Peng, H. *Acta. Chim. Sinica* **2012**, *70*, 1523.

DOI: 10.1021/jacs.5b10131
J. Am. Chem. Soc. 2016, 138, 225−230